Journal of Process Control 21 (2011) 652–666

Contents lists available at ScienceDirect

Journal of Process Control

journal homepage: www.elsevier.com/locate/jprocont

A comparison of nonlinear observers for output feedback model-based control of seeded batch crystallization processes

Ali Mesbah[a,b,*], Adrie E.M. Huesman[a], Herman J.M. Kramer[b], Paul M.J. Van den Hof[a]

[a] Delft Center for Systems and Control, Delft University of Technology, Mekelweg 2, 2628 CD, Delft, The Netherlands
[b] Process and Energy Laboratory, Delft University of Technology, Leeghwaterstraat 44, 2628 CA, Delft, The Netherlands

ARTICLE INFO

Article history:
Received 8 May 2010
Received in revised form
22 November 2010
Accepted 23 November 2010
Available online 19 January 2011

Keywords:
Batch crystallization
Population balance equation
Nonlinear model-based control
State estimation
Kalman filters
Moving horizon estimator

ABSTRACT

This paper presents a comparative analysis of various nonlinear estimation techniques when applied for output feedback model-based control of batch crystallization processes. Several nonlinear observers, namely an extended Luenberger observer, an extended Kalman filter, an unscented Kalman filter, an ensemble Kalman filer and a moving horizon estimator are used for closed-loop control of a semi-industrial fed-batch crystallizer. The performance of the nonlinear observers is evaluated in terms of their closed-loop behavior as well as their ability to cope with model imperfections and process uncertainties such as measurement errors and uncertain initial conditions. The simulation results suggest that the extended Kalman filter and the unscented Kalman filter provide accurate state estimates that ensure adequate fulfillment of the control objective. The results also confirm that adopting a time-varying process noise covariance matrix further enhances the estimation accuracy of the latter observers at the expense of a slight increase in their computational burden. This tuning method is particularly suited for batch processes as the state variables often vary significantly along the batch run. It is observed that model imperfections and process uncertainties are largely detrimental to the accuracy of state estimates. The degradation in the closed-loop control performance arisen from inadequate state estimation is effectively suppressed by the inclusion of a disturbance model into the observers.

1. Introduction

Batch crystallization is extensively utilized in the pharmaceutical, food and fine chemical industries for the production of high value-added specialty chemicals. Model-based control and performance monitoring of these processes typically require knowledge of the system states. In most crystallization applications, measurements of crystal size distribution (CSD) and solute concentration, along with temperature, are essential. Despite the advent of process analytical technology in recent years [7], online measurement of all process variables is not often viable due to various technological and economical limitations. Several challenges yet exist in reliable measurement of the evolution of CSD and solute concentration during a batch crystallization process. The merits and demerits of online sensors commonly utilized for measuring CSD and solute concentration have been extensively investigated in the literature; see, e.g. [50,30] and the references therein.

In theory, the unmeasurable process variables can be estimated by real time simulation of a crystallization model in parallel to the process. However, process models typically exhibit structural and parametric mismatch with respect to the real process. The model imperfections, alongside uncertain initial conditions, unmeasured process disturbances and measurement errors, tend to degrade the quality of the estimated process variables. A remedy for this deficiency is the use of state observers that combine information from two sources, namely a process model and available online measurements, to estimate the states of a dynamic system in real time.

A wide variety of approaches for state estimation of nonlinear dynamic systems have been proposed in the literature. The nonlinear state observers commonly used in (bio)chemical process applications can be categorized into exponential and asymptotic estimation techniques [3]. The former class of observers assumes a perfect knowledge of the model structure including the process kinetics, whereas the asymptotic observers merely rely on conservation laws without requiring the knowledge of process kinetics. Thus, the great deal of uncertainty associated with the kinetic parameters is eliminated in the asymptotic observers. However, this is achieved at the expense of a convergence rate that is fully governed by the process conditions, while the adjustable rate of convergence of the exponential observers is determined by tuning parameters [15]. To overcome the shortcomings of these estima-

* Corresponding author at: Delft Center for Systems and Control, Delft University of Technology, Mekelweg 2, 2628 CD, Delft, The Netherlands.
E-mail address: ali.mesbah@tudelft.nl (A. Mesbah).

0959-1524/$ – see front matter © 2010 Elsevier Ltd. All rights reserved.
doi:10.1016/j.jprocont.2010.11.013

tion techniques, several hybrid state estimators have recently been proposed. These observers evolve between an exponential and an asymptotic observer in accordance with the quality of the kinetic model [6,26,39]. A more common approach is however the use of the so-called adaptive exponential observers that combine the state observation with the estimation of the poorly known parameters [2,10,15,49,52,53,68].

The most widely used variant of the exponential observers is the extended Kalman filter (EKF). The EKF may result in significant estimation errors when the system is highly nonlinear or the state probability distribution functions (pdfs) are nonGaussian. To alleviate the drawbacks of the EKF, derivative free stochastic observers, namely the unscented Kalman filter (UKF) [29] and Monte Carlo filters [21] have been developed. While the state pdfs are yet assumed to be Gaussian, the UKF avoids linearization of the system model through an unscented transformation. As a result, the UKF is capable of estimating the state pdfs with a higher accuracy in addition to circumventing the need for computing the Jacobian matrices. On the other hand, the Monte Carlo filters have found widespread use owing to the ever increasing computing power. These filters are capable of dealing with nonlinear state estimation problems with multimodal and nonGaussian pdfs [1]. As reported in [13], there is a large variety of Monte Carlo filters, which use Monte Carlo simulation techniques to implement the recursive Bayesian estimation framework. The merit of the Monte Carlo filters lies in their ability to handle nonlinear process dynamics without making any assumptions neither on the nature of dynamics nor on the shape or any other characteristics of pdfs.

It is well-known that (bio)chemical processes are often subject to constraints due to various operational and economical considerations. Optimization-based state estimation, which enables explicit inclusion of constraints into the nonlinear estimation problem, has become an active research area in recent years [18,23,55,58,65,70]. A historical review on the developments of this approach is given in [57]. The nonlinear optimization-based estimation techniques can be classified as full information or moving horizon estimators [59]. The estimation horizon of the full information estimators grows as new measurements become available, whereas in the moving horizon estimators the optimization is performed over a finite time horizon to avoid excessively large computational burdens. In general, the optimization-based observers need not any assumptions neither on the state pdfs nor on the noise sequences acting on the system.

Another class of nonlinear state estimation techniques known as the high gain observers has also received substantial attention in the literature [2,5,11,14,19]. The high gain observers are based on the notion of linearization through coordinate transformation [68]. These observers tend to possess similar characteristics as the extended Luenberger observer and the extended Kalman filter [15].

This study is intended to investigate the effectiveness of various nonlinear observers for output feedback model-based control of industrial batch crystallization processes. Successful implementation of a model-based control strategy largely relies on the estimation quality of current states of the system, which are utilized to make predictions of the system behavior in future. Thus far, the extended Luenberger observer and the extended Kalman filter have been the most widely used techniques for nonlinear state estimation in batch crystallization processes [36,38,43,45,48,66,74,76]. However, the inherent shortcomings of these observers in coping with the nonlinear dynamics of crystallization systems that are subject to large disturbances necessitate the recourse to estimation techniques, which better suit the characteristics of batch crystallization processes.

This paper provides a comparative performance analysis of various nonlinear estimation techniques when applied for online control of industrial batch crystallizers. Several state estimation techniques, namely the extended Luenberger technique, the extended Kalman filtering, the unscented Kalman filtering, the ensemble Kalman filtering [16] belonging to the broader class of Monte Carlo filters and the moving horizon estimation technique, are used to develop nonlinear state observers for a semi-industrial batch crystallizer. In addition to open-loop tests, the nonlinear observers are embedded in an output feedback model-based control framework. This facilitates performance evaluation of the observers in terms of their closed-loop behavior as well as their ability to cope with model imperfections and process uncertainties commonly encountered in industrial batch crystallizers. The process uncertainties include uncertain initial conditions, unmeasured process disturbances and measurement errors.

The paper is organized as follows. In Section 2, the principles and algorithms of the nonlinear state estimators are discussed. Section 3 presents the semi-industrial fed-batch crystallizer, for which the observers are developed, along with the description of the process model. This is followed by the observability analysis of the system at hand and the simulation results of various scenarios, under which the open-loop and closed-loop performance of the observers is evaluated. Finally, the concluding remarks are given in Section 4.

2. Nonlinear state estimation techniques

The class of nonlinear systems of interest is formulated in a discrete-time state space form

$$\begin{aligned} x_k &= f(x_{k-1}, u_{k-1}, w_{k-1}) \\ y_k &= h(x_k, u_k, v_k), \end{aligned} \tag{1}$$

where x_k is the vector of state variables, whose initial values are random variables with a given pdf; u_k is the vector of measured process inputs, which are assumed to be constant over the time interval $[t_{k-1}, t_k]$; y_k is the vector of output measurements; $f(x_{k-1}, u_{k-1}, w_{k-1})$ is the nonlinear process model that is generally the solution of a system of differential algebraic equations (DAE) over the time interval $[t_{k-1}, t_k]$; $h(x_k, u_k, v_k)$ is a possibly nonlinear measurement model; w_k is the vector of process noise with $\mathbb{E}[w_k] = 0$ and $\mathbb{E}[w_k w_k^T] = Q_k$; v_k is the vector of measurement noise with $\mathbb{E}[v_k] = 0$ and $\mathbb{E}[v_k v_k^T] = R_k$.

Given a process model and a sequence of noisy process measurements, the observer aims to estimate the state vector. In the following, the algorithms of the nonlinear state estimation techniques considered in this work are briefly presented.

2.1. Extended Luenberger observer

Zeitz [75] was the first to introduce the extended Luenberger observer (ELO) based on the work of Krener and Isidori [35] on nonlinear observers. For a deterministic system, i.e. $w = 0$ and $v = 0$, a Luenberger-type observer can be established as

$$\hat{x}_{k+1} = f(\hat{x}_k, u_k) + K_k(y_k - h(\hat{x}_k)), \tag{2}$$

where $\hat{x}_k$ is an estimate of the state vector and K_k is the observer gain that determines the convergence properties of the state estimator. Eq. (2) indicates that the observer equation consists of two parts, namely a copy of the process model and a correction term that is the difference between the estimated and measured output variables multiplied by the gain matrix.

The goal of the ELO is to provide an estimate of the state vector such that the observation error

$$\begin{aligned} e_{k+1} &= x_{k+1} - \hat{x}_{k+1} = f(\hat{x}_k + e_k, u_k) - f(\hat{x}_k, u_k) \\ &\quad - K_k(h(\hat{x}_k + e_k) - h(\hat{x}_k)), \end{aligned} \tag{3}$$

is minimal. For nonlinear systems a condition, under which the error converges to zero, cannot be readily deduced from the error

dynamics. This implies that the observer gain needs to be determined on the basis of a linearized version of the original process model. Thus, linearizing the nonlinear model around $e=0$ yields [15]

$$e_{k+1} = (A_k - K_k C_k)e_k, \tag{4}$$

where $A_k = [\partial f(x_k, u_k)/\partial x]_{x_k=\hat{x}_k}$ and $C_k = [\partial h(x_k, u_k)/\partial x]_{x_k=\hat{x}_k}$ are the linear approximations of the nonlinear process dynamics, i.e. Eq. (1), around the estimated state vector $\hat{x}_k$. The choice of the time-varying observer gain K_k relies on local stability properties of the state estimator. The gain should be chosen such that the linearized error dynamics are asymptotically stable.

In general, the estimation accuracy of the ELO largely depends on how well the linearized model represents the nonlinear dynamics. Initialization of the observer is also crucial since accurate linearization of process and measurement functions around $e=0$ requires that the observer is initialized sufficiently close to the true states. Several studies on successful application of the ELO for closed-loop control of batch crystallization processes have been reported in the literature [36,42,66]. The applied observers are mostly high gain extended Luenberger observers [11]. The structure of the gain matrix is defined on the basis of physical insights into the process, while its tuning parameters are obtained by running open-loop simulations and evaluating the evolution of the states.

2.2. Extended Kalman filter

The Kalman filter calculates the minimum variance estimates of the state vector in an optimal probabilistic setting [33]. This notion can be extended to systems with nonlinear dynamics, whose models are differentiable. The EKF applies the optimal Kalman theory to a linear approximation of the nonlinear system. The covariance of the state pdfs is propagated through a linear approximation of the process model obtained around the operating point at each time instant using a Taylor series expansion. The EKF requires that the initial state variables x_0 and the noise sequences acting on the system, i.e. w and v, to be random variables with Gaussian distributions. These pdfs are however no longer Gaussian when undergoing nonlinear transformations. Thus, the EKF presents a suboptimal solution to the state estimation problem of nonlinear systems since it assumes that the random variables still retain their Gaussian pdfs after the transformation.

The EKF has a recursive algorithm consisting of two parts, namely the prediction stage and the measurement correction stage. In the former stage, the a priori state estimates $\hat{x}_{k+1|k}$ and their associated error $P_{k+1|k}$ are determined by propagating the mean $\hat{x}_{k|k}$ and the covariance $P_{k|k}$ of the state pdfs at the preceding time step through the nonlinear process model and its first order linearization, respectively,

$$\begin{aligned} \hat{x}_{k+1|k} &= f(\hat{x}_{k|k}, u_k, w_k) \\ P_{k+1|k} &= F_k P_{k|k} F_k^T + W_k Q_k W_k^T, \end{aligned} \tag{5}$$

where $F_k = [\partial f(x_k, u_k, w_k)/\partial x]_{x_k=\hat{x}_{k|k}}$ and $W_k = [\partial f(x_k, u_k, w_k)/\partial w]_{x_k=\hat{x}_{k|k}}$. Subsequently, in the measurement correction stage the a posteriori state estimates $\hat{x}_{k+1|k+1}$ and the a posteriori error $P_{k+1|k+1}$ are calculated using current measurements y_k

$$\begin{aligned} \hat{x}_{k+1|k+1} &= \hat{x}_{k+1|k} + K_k(y_k - h(\hat{x}_{k+1|k}, u_k, v_k)) \\ P_{k+1|k+1} &= (I - K_k H_k)P_{k+1|k}. \end{aligned} \tag{6}$$

K_k is the Kalman filter gain defined as

$$K_k = P_{k+1|k} H_k^T (H_k P_{k+1|k} H_k^T + V_k R_k V_k^T)^{-1}, \tag{7}$$

in which $H_k = [\partial h(x_k, u_k, v_k)/\partial x]_{x_k=\hat{x}_{k+1|k}}$ and $V_k = [\partial h(x_k, u_k, v_k)/\partial v]_{x_k=\hat{x}_{k+1|k}}$.

Amongst the various nonlinear observers, the EKF is the most widely used state estimation technique in diverse process control applications. This is due to its relatively easy implementation and limited computational burden; e.g. see [68,15] and the references therein. The EKF however suffers from several practical shortcomings, namely its inapplicability to highly nonlinear, nondifferentiable systems, difficult tuning and inability to systematically incorporate state constraints. A critical evaluation of the extended Kalman filter is given in [73], where the authors have raised their serious doubts on the usefulness of the EKF in industrial applications. Nonetheless, owing to its low computational burden, the EKF has been extensively utilized for model-based control of various processes [4,37,69], including batch crystallization processes [36,48,74,76]. These studies indicate that successful implementation of the EKF in a nonlinear model predictive control scheme largely relies on the accuracy of model approximations and the initial estimate of the state vector.

2.3. Unscented Kalman filter

The unscented Kalman filter is primarily developed to alleviate the main deficiency of the EKF, namely linear approximation of the nonlinearities, by applying the unscented transformation to the Kalman estimation notion. The underlying idea of the UKF is to approximate the Gaussian state PDFs by a number of deterministically chosen points, the so-called sigma points, such that their mean and covariance match those of the distribution [28,29]. These points are then propagated through the nonlinear system model to determine expectations and covariances of the state estimates. Clearly, this is in contrast to the EKF that propagates only a single point through a linearized version of the original system model.

The filter algorithm is defined on the basis of the same steps as in the EKF. A set of $2n+1$ symmetric sigma points, where n denotes the dimension of the state vector, is generated around the means of the set with a distance of the square root of the covariances. Once the sigma points are chosen, they are propagated through the nonlinear model equations to calculate the a priori mean and covariance of the state vector from the transformed set of points

$$\begin{aligned} \chi_{k+1}^i &= f(\chi_k^i, u_k, w_k) \\ \hat{x}_{k+1|k} &= \sum_{i=1}^{2n+1} \alpha_i \chi_{k+1}^i \\ P_{k+1|k} &= \sum_{i=1}^{2n+1} \alpha_i [\chi_{k+1}^i - \hat{x}_{k+1|k}][\chi_{k+1}^i - \hat{x}_{k+1|k}]^T + Q_k, \end{aligned} \tag{8}$$

where α_i denotes the weighting coefficients. It is evident that the prediction stage differs from the EKF in that the nonlinear process model is not linearized. Instead, the UKF propagates a cluster of points, centered around the current state estimates, to more accurately approximate the covariance of the state pdfs. The a priori state vector and its associated covariance are then updated using measurements

y_k

$$\begin{aligned}
\gamma^i_{k+1} &= h(\chi^i_k, u_k, v_k)\\
\hat{y}_{k+1|k} &= \sum_{i=1}^{2n+1}\alpha_i\gamma^i_{k+1}\\
P_{yy,k+1|k} &= \sum_{i=1}^{2n+1}\alpha_i[\gamma^i_{k+1}-\hat{y}_{k+1|k}][\gamma^i_{k+1}-\hat{y}_{k+1|k}]^T + R_k\\
P_{xy,k+1|k} &= \sum_{i=1}^{2n+1}\alpha_i[\chi^i_{k+1}-\hat{x}_{k+1|k}][\gamma^i_{k+1}-\hat{y}_{k+1|k}]^T\\
K_k &= P_{xy,k+1|k}P^{-1}_{yy,k+1|k}\\
\hat{x}_{k+1|k+1} &= \hat{x}_{k+1|k} + K_k(y_k-\hat{y}_{k+1|k})\\
P_{k+1|k+1} &= P_{k+1|k} - K_kP_{yy,k+1|k}K_k^T.
\end{aligned} \tag{9}$$

In addition to its easy implementation, the unscented Kalman filter provides at least second order accuracy for the mean value and covariance approximations, whereas the EKF is only accurate up to the first order moment of the pdfs [28]. The computational efficiency of the UKF is comparable to that of the EKF; generally being in the order of $O(n^3)$ operations, provided that the dimension of the state vector is large compared to the number of measurements, i.e. the dimension of y_k. Some variants of the UKF such as the square root unscented Kalman filter [72] can be implemented using $O(n^2)$ operations. Hao et al. [22] presented a comparative analysis of several computationally efficient types of the UKF obtained for systems exhibiting certain characteristics, e.g. linear measurement function, additive type noise, etc.

Several studies on open-loop implementation of the UKF in process control applications have been reported [34,55,62,63,65]. However, the UKF has rarely been applied to crystallization processes. Mangold et al. [41] employed a square root unscented Kalman filter to estimate the particle size distribution of barium sulphate in a semi-batch precipitator. A population balance model was used to describe the process dynamics. Despite the promising results, closed-loop implementation of the UKF remained to be investigated. More recently, Hermanto et al. [24] designed an UKF for nonlinear model predictive control of polymorphic transformation of L-glutamic acid crystals. The simulation results indicate that the UKF provides adequate state estimates that lead to a good overall closed-loop control performance.

2.4. Ensemble Kalman filter

Contrary to the UKF, the ensemble Kalman filter (EnKF) constitutes a class of derivative free nonlinear filters that can cope with multimodal and nonGaussian distributions [9,16]. The EnKF is a suboptimal estimator, where the error statistics are predicted by solving the Fokker–Planck equation by means of a Monte Carlo method; the Fokker–Planck equation governs the time evolution of the state pdfs. This is in contrast to the EKF, in which the error statistics are calculated using the approximate error covariance equation. The underlying notion of the EnKF is to represent the state pdfs by a large ensemble of randomly chosen points to describe all statistical properties of the state variables. Integrating the ensemble members forward in time according to the stochastic system dynamics is equivalent to solving the Fokker–Planck equation using a Monte Carlo method.

In the prediction stage of the filter algorithm, a set of sample points, i.e. $\hat{x}^i_{k|k}$, that describes the statistics of the state pdfs is generated using a Monte Carlo sampling technique. The sample points are propagated through the nonlinear system to compute a cloud of transformed sample points

$$\hat{x}^i_{k+1|k} = f(\hat{x}^i_{k|k}, u_k, w_k). \tag{10}$$

These sample points are then used to estimate the a priori sample mean and error covariance matrices

$$\begin{aligned}
\bar{x}_{k+1|k} &= \frac{1}{N}\sum_{i=1}^{N}\hat{x}^i_{k+1|k}\\
\bar{y}_{k+1|k} &= \frac{1}{N}\sum_{i=1}^{N}h(\hat{x}^i_{k+1|k}, u_k, v_k)\\
E_{x_{k+1|k}} &= [\hat{x}^1_{k+1|k}-\bar{x}_{k+1|k}\cdots\hat{x}^N_{k+1|k}-\bar{x}_{k+1|k}]\\
E_{y_{k+1|k}} &= [\hat{y}^1_{k+1|k}-\bar{y}_{k+1|k}\cdots\hat{y}^N_{k+1|k}-\bar{y}_{k+1|k}]\\
P_{xy,k+1|k} &= \frac{1}{N-1}E_{x_{k+1|k}}E^T_{y_{k+1|k}}\\
P_{yy,k+1|k} &= \frac{1}{N-1}E_{y_{k+1|k}}E^T_{y_{k+1|k}} + R_k.
\end{aligned} \tag{11}$$

It is evident from Eq. (11) that the prediction error covariance matrices are defined around the ensemble mean. This implies that the ensemble mean provides the best prediction estimate of the state variable and the spread of ensemble members around the mean is a natural definition of the error of the ensemble mean. Finally, the EnKF performs an ensemble of parallel data assimilation steps to obtain the a posteriori state estimates

$$\begin{aligned}
K_k &= P_{xy,k+1|k}P^{-1}_{yy,k+1|k}\\
\hat{x}^i_{k+1|k+1} &= \hat{x}^i_{k+1|k} + K_k(y_k - h(\hat{x}^i_{k+1|k}, u_k, v_k))\\
\bar{x}_{k+1|k+1} &= \frac{1}{N}\sum_{i=1}^{N}\hat{x}^i_{k+1|k+1}.
\end{aligned} \tag{12}$$

Note that the process and measurement noise vectors may have arbitrary, but known distributions.

The computational cost of the EnKF is in the order of $O(pNn)$ operations, where p is the number of outputs of the system, N is the ensemble size and n is the dimension of the state vector [20]. Thus, if $N \ll n$, the computational burden of evaluating the approximate covariances in the EnKF will be less than that required by the EKF. When N is large, the EnKF may however become computationally too expensive since the model needs to be simulated N times.

The EnKF has been used in several applications such as meteorology [25], oceanography [64] and reservoir engineering [27]. In these applications, the nonlinear models are of extremely high order, the initial states are highly uncertain and a large number of measurements are usually available. The EnKF is particularly advantageous when dealing with such large size problems since a number of ensembles of about 50–100 are often sufficient to describe the dynamics of systems with thousands of states. Nonetheless, the use of the EnKF in process applications has received little attention. Gillijns et al. [20] applied the EnKF to estimate the states of a compressible fluid flow in a one dimensional channel. They showed that the ensemble Kalman filter provides fairly accurate state estimates once a threshold ensemble size is reached. Prakash et al. [54] presented a constrained recursive formulation of the EnKF, which systematically deals with bounds on the states. The effectiveness of the proposed algorithm is demonstrated by its application to a simulated gas-phase reactor. The performance evaluation of the EnKF in the latter studies is based merely on open-loop simulations. To our knowledge, the closed-loop performance of the ensemble Kalman filter in process applications, e.g. crystallization processes, has not been explored thus far.

2.5. Moving horizon estimator

What distinguishes the moving horizon estimator (MHE) from other estimation techniques is its ability to incorporate constraints into the estimation problem. The MHE is an optimization-based estimator, wherein the state estimates are obtained by solving a minimization problem, e.g. the sum of squared errors, while the nonlinear model equations and constraints of different kinds are fulfilled [60]. In optimization-based estimators, the objective function is intended to indicate the accuracy of model predictions with respect to process outputs obtained over a certain time interval. In contrast to the classical state estimators, which only utilize the most recent measurements to update the model predictions, the MHE uses measurements gathered over a predetermined time horizon for the observer correction. The latter characteristic of optimization-based estimators typically makes them computationally more expensive than stochastic observers.

The moving horizon estimation problem can be stated in its most general form as the solution of the following optimization problem [57]

$$\begin{aligned} &\min_{x_{T-P},\{w_k\}_{k=T-P}^{T-1}} \sum_{k=T-P}^{T-1} ||v_k||^2_{R^{-1}} + ||w_k||^2_{Q^{-1}} + Z_{T-P}(x_{T-P}) \\ &\text{subject to :} \quad \text{Eq. (1)} \\ &x_k \in X, \quad w_k \in W, \quad v_k \in V, \end{aligned} \tag{13}$$

where the sets X, W and V can be constrained; P is the horizon size. To ensure the feasibility of the optimization problem, measurement noise constraints are often avoided. Eq. (13) implies that the last P measurements are explicitly used to solve the optimal estimation problem over the time horizon $T-P \le k \le T-1$. The remaining process measurements are accounted for by function $Z_{T-P}(x_{T-P})$, the so-called arrival cost term, which summarizes the effect of prior measurement information on the state estimates obtained at time instant $T-P$. The arrival cost term facilitates the transformation of an infinite dimensional optimization problem into one of the finite dimension by providing a means to compress the data. Exact algebraic expressions for the arrival cost term only exist for unconstrained linear systems with Gaussian pdfs. Under these conditions, the moving horizon estimator reduces to the Kalman filter [60]. In the case of constrained nonlinear systems, the arrival cost term needs to be approximated, e.g. using a first order Taylor series approximation of the model around the estimated trajectory as in the EKF or by evaluating sigma points as in the UKF. The approximation allows us to compute the error covariance of the estimated states at time instant $T-P$. Adequate approximation of the arrival cost term is crucial to guaranteeing the stability and performance of the MHE.

The moving horizon estimator has received considerable attention in model-based process control applications due to the duality between constrained estimation and control, e.g. see [40,65,70]. A few applications of the optimization-based estimators in crystallization processes have also been reported in the literature. Mangold et al. [41] applied the moving horizon estimation technique to a population balance model to estimate the evolution of particle size distribution in semi-batch precipitation of barium sulphate. The performance of the MHE was evaluated against a square root unscented Kalman filter on the basis of several open-loop simulations. The results suggest that the MHE is slightly more robust to large uncertainties in the initial conditions of the estimator, whereas the unscented Kalman filter outperforms the optimization-based estimator when the measurement data is noisy. Recently, Nagy [46] presented a nonlinear model predictive control scheme to robustly design the shape of crystal size distribution in batch crystallization processes. To facilitate real-time implementation of the model-based control framework, a moving horizon estimator is utilized to estimate the crystal conversion shape parameter based on online chord length distribution measurements. The simulation and experimental results indicate adequate estimation of the latter parameter by the optimization-based estimator.

3. Case study: a semi-industrial fed-batch evaporative crystallizer

The above discussed estimation techniques are used to design nonlinear observers for seeded fed-batch evaporative crystallization of an ammonium sulphate–water system. The crystallization takes place in a 75-l draft tube crystallizer. The semi-industrial crystallizer is considered as a single well-mixed compartment with one inlet and two outlet streams. The fed-batch operation is exercised to compensate for losses in the crystallization volume due to the evaporation of solvent, i.e. water, and the slurry sampling. Therefore, the crystallizer is continuously fed throughout the batch run with a crystal-free feed stream containing saturated ammonium sulphate solution. On the other hand, the outlet flows from the crystallizer include an unclassified product removal stream as well as a vapor stream that is free from crystal and solute. The small product flow is withdrawn from the crystallizer at regular time intervals every 100 s. The product flow is diluted with the saturated feed solution for 20 s to facilitate online measurement of CSD with a laser diffraction instrument (HELOS-Vario, Sympatec, Germany). Neumann and Kramer [50] demonstrated that the evolution of CSD in industrial crystallizers can be adequately measured on the basis of the laser diffraction principle when the solid concentration is low, i.e. 1.5 vol.%. It should be noted that seeding is carried out to ensure the reproducibility of batch runs and the achievement of the desired product quality specifications. The batch runs are initiated by inserting certain amounts of ground seeds of a known sieve fraction into the crystallizer [32].

3.1. Model development

The dynamic behavior of a solution crystallization process can be represented by the population balance equation, along with conservation balance equations and kinetic relations. The population balance equation describes the evolution of number of crystals along the temporal and size domains. The method of moments [56] can be applied to recast the population balance equation into a set of computationally affordable ordinary differential equations. This approach reduces the detailed information on the full crystal size distribution that is provided by the population balance equation. Hence, the method of moments allows us to calculate only the relevant properties of the total crystal population required for the intended control application. For the system under study, the evolution of the moments of CSD in time is expressed as

$$\frac{dm_i}{dt} = 0^i B_0 + iGm_{i-1} - \frac{m_i Q_p}{V}, \qquad m_i(t_0) = m_{i,0}, \quad i = 0, \ldots, 4, \tag{14}$$

where m_i is the ith moment of crystal size distribution ($\mathrm{m}^i/\mathrm{m}^3$); G is the crystal growth rate (m/s); B_0 is the total nucleation rate ($\#/\mathrm{m}^3/\mathrm{s}$); t is the time (s); V is the crystallizer volume (m^3); Q_p is the unclassified product removal flow rate (m^3/s). The four leading moments of CSD have physical significations: m_0 represents the total number of crystals, m_1 represents the total length of crystals, m_2 is proportional to the total crystal surface area and m_3 is proportional to the total crystal volume. m_4 is used to calculate the mean crystal size, i.e. the ratio of m_4 to m_3.

The particle formation is attributed to secondary nucleation from crystal surfaces since it is often the most dominant nucleation

Table 1
Model parameters and physical properties of the ammonium sulphate–water crystallizing system.

Parameter	Value
C^* ($kg_{solute}/kg_{solution}$)	0.46
g	1.0
H_c (kJ/kg)	60.75
H_L (kJ/kg)	69.86
H_v (kJ/kg)	2.59×10^3
K_v	0.43
k_b (#/m^4)	1.02×10^{14}
k_g (m/s)	7.50×10^{-5}
Q_p (m^3/s)	1.73×10^{-6}
V (m^3)	7.50×10^{-2}
ρ_c (kg/m^3)	1767.35
ρ_L (kg/m^3)	1248.93

mechanism occurring in seeded batch crystallizers. The empirical expressions realized for the total nucleation rate and the size-independent crystal growth rate are [12]

$$B_0 = k_b m_3 G \tag{15}$$

$$G = k_g (C - C^*)^g. \tag{16}$$

The nucleation rate constant k_b, the crystal growth rate constant k_g and the crystal growth rate exponent g are the kinetic parameters specific to the ammonium sulphate–water crystallizing system. Furthermore, C and C^* are the solute concentration and the saturation concentration, respectively, whose difference determines the driving force, namely the supersaturation, of the crystallization process.

Due to the isothermal operation of the evaporative crystallizer, the mass and energy balance equations simplify to a single expression for the solute concentration

$$\frac{dC}{dt} = \frac{(Q_p(C^* - C)/V) + 3K_v G m_2 (k_1 + C)}{1 - K_v m_3} + \frac{k_2 H_{in}}{1 - K_v m_3} \quad C(t_0) = C_0 \tag{17}$$

with the constant coefficients

$$k_1 = \frac{H_v C^*}{H_v - H_L} \left(\frac{\rho_c}{\rho_L} - 1 + \frac{\rho_L H_L - \rho_c H_c}{\rho_L H_v} \right) - \frac{\rho_c}{\rho_L} \tag{18}$$

$$k_2 = \frac{C^*}{V \rho_L (H_v - H_L)}, \tag{19}$$

where K_v is the crystal volumetric shape factor; H_{in} is the heat input to the crystallizer (kW); ρ_L is the density of saturated solution (kg/m^3); ρ_c is the density of crystals (kg/m^3). H_L, H_c and H_v are the solution, crystal and vapor specific enthalpies (kJ/kg), respectively. The model parameters and physical properties of the ammonium sulphate–water crystallizing system are listed in Table 1. As has been discussed in [44], the nonlinear moment model provides an adequate description of the process at hand.

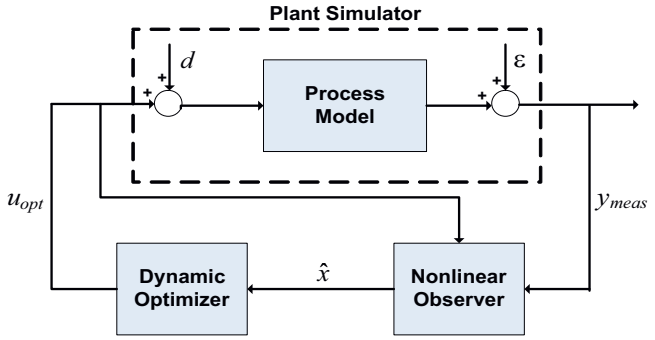

Fig. 1. The output feedback nonlinear model-based control framework.

To develop the nonlinear observers, the model equations are recast as a smooth affine control system

$$\begin{aligned} \dot{x} &= \mathcal{F}(x) + \mathcal{G}(x)u \\ y_i &= \mathcal{H}_i(x), \quad i = 1, 2, \ldots, 5, \end{aligned} \tag{20}$$

where the system states $x = (m_0, \ldots, m_4, C)$ constitute the local coordinates for a smooth manifold M, namely the state space manifold; $u = H_{in} \in U \subset \mathbb{R}$ is the input to the system; $\mathcal{F}$ and $\mathcal{G}$ are smooth vector fields on M; $\mathcal{H} : M \to \mathbb{R}^5$ is the smooth output map of the system. The vector fields of the smooth affine control system are defined as

$$\mathcal{F} = \begin{pmatrix} k_b m_3 k_g (C - C^*)^g - \dfrac{m_0 Q_p}{V} \\ k_g (C - C^*)^g m_0 - \dfrac{m_1 Q_p}{V} \\ 2k_g (C - C^*)^g m_1 - \dfrac{m_2 Q_p}{V} \\ 3k_g (C - C^*)^g m_2 - \dfrac{m_3 Q_p}{V} \\ 4k_g (C - C^*)^g m_3 - \dfrac{m_4 Q_p}{V} \\ \dfrac{(Q_p(C^* - C)/V) + 3K_v k_g (C - C^*)^g m_2 (k_1 + C)}{1 - K_v m_3} \end{pmatrix},$$

$$\mathcal{G} = \begin{pmatrix} 0 \\ 0 \\ 0 \\ 0 \\ 0 \\ \dfrac{k_2}{1 - K_v m_3} \end{pmatrix} \quad \text{and} \quad \mathcal{H} = \begin{pmatrix} m_0 \\ m_1 \\ m_2 \\ m_3 \\ m_4 \end{pmatrix}. \tag{21}$$

Note that the smooth output map of the system, i.e. $\mathcal{H} : \mathbb{R}^6 \to \mathbb{R}^5$, only consists of the five leading moments of CSD.

3.2. Observability analysis

According to Nijmeijer and van der Schaft [51], the observation space O of a nonlinear system of the form given in Eq. (20) is the linear space (over $\mathbb{R}$) of functions on M containing $\mathcal{H}_1, \ldots, \mathcal{H}_5$ and all repeated Lie derivatives

$$L_{z_1} L_{z_2} \ldots L_{z_k} \mathcal{H}_j, \qquad j = 1, \ldots, 5, \quad k = 1, 2, \ldots \tag{22}$$

with z_i, $i \in k$ in the set $\{\mathcal{F}, \mathcal{G}\}$. The observation space O defines the observability codistribution O_c by setting $O_c = dO$, i.e.

$$\begin{aligned} O_c = \operatorname{span}\{&d\mathcal{H}_1(x_0), \ldots, d\mathcal{H}_p(x_0), dL_{z_1} L_{z_2} \ldots L_{z_k} \mathcal{H}_j(x_0)\}, \\ &j = 1, \ldots, 5, \quad k = 1, 2, \ldots. \end{aligned} \tag{23}$$

It can be stated that the nonlinear system given in Eq. (20) with $\dim M = n$ is locally observable at x_0 if

$$\dim(O_c(x_0)) = n. \tag{24}$$

Accordingly, the codistribution for the system under study is defined as

$$O_c = \begin{pmatrix} 1 & 0 & 0 & 0 & 0 & 0 \\ 0 & 1 & 0 & 0 & 0 & 0 \\ 0 & 0 & 1 & 0 & 0 & 0 \\ 0 & 0 & 0 & 1 & 0 & 0 \\ 0 & 0 & 0 & 0 & 1 & 0 \\ -\dfrac{Q_p}{V} & 0 & 0 & k_b k_g (C - C^*)^g & 0 & k_b k_g m_3 g (C - C^*)^{g-1} \end{pmatrix}. \tag{25}$$

It is evident that the codistribution has a full rank of 6 when $(C - C^*)$ is not zero. Thus, the system is locally observable since the rank of O_c is equal to the number of system states.

3.3. Closed-loop performance analysis

To evaluate the closed-loop performance of the nonlinear state estimation techniques, the observers are embedded in an output feedback model-based control framework [42]. The core component of the online control strategy is an optimal control problem formulated as

$$\min_{H_{in}(t)} \frac{\int_0^{t_f} (100(G(t) - G_{\max})/G_{\max})^2 dt}{\int_0^{t_f} dt} \quad (26)$$
$$\text{subject to : Eqs.(14)–(19)}$$
$$H_{\min} \le H_{in}(t) \le H_{\max},$$

where $H_{in}(t)$ is the parameterized heat input profile; t_f is the batch time; $G_{\max}$ is the maximum admissible crystal growth rate to circumvent the formation of irregularly shaped crystals and to limit the detrimental effects of high supersaturation on the product quality ($G_{\max} = 2.5 \times 10^{-8}\, m/s$). Eq. (26) seeks a trade-off between the fulfillment of product quality requirements and the maximization

Table 2
Computation times of the nonlinear observers.

Nonlinear observer	Average CPU-time[a] of one iteration (s)
ELO	0.012
EKF	0.012
EKF (time-varying Q)	0.013
UKF	0.032
UKF (time-varying Q)	0.033
EnKF (ensemble size: 10)	0.087
EnKF (ensemble size: 20)	0.157
EnKF (ensemble size: 40)	0.297
EnKF (ensemble size: 80)	0.581
MHE (estimation horizon: 300 s)	0.610
MHE (estimation horizon: 500 s)	0.629
MHE (estimation horizon: 700 s)	0.658

[a] The reported CPU-times correspond to the Microsoft Windows XP (Professional) operating system running on a Genuine Intel (R) T2050 @1.60 GHz processor with 1 GB RAM.

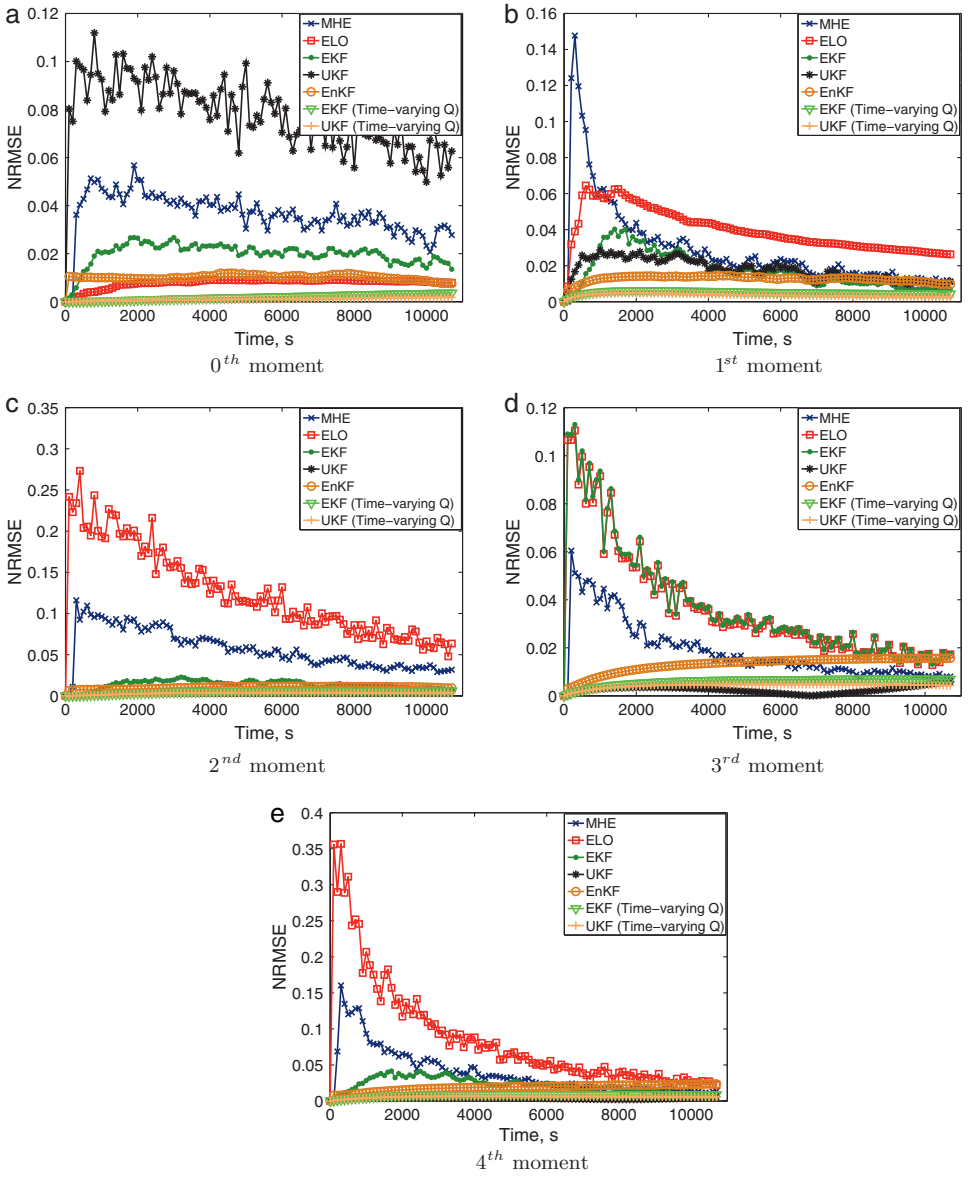

Fig. 2. State estimation errors under the nominal scenario.

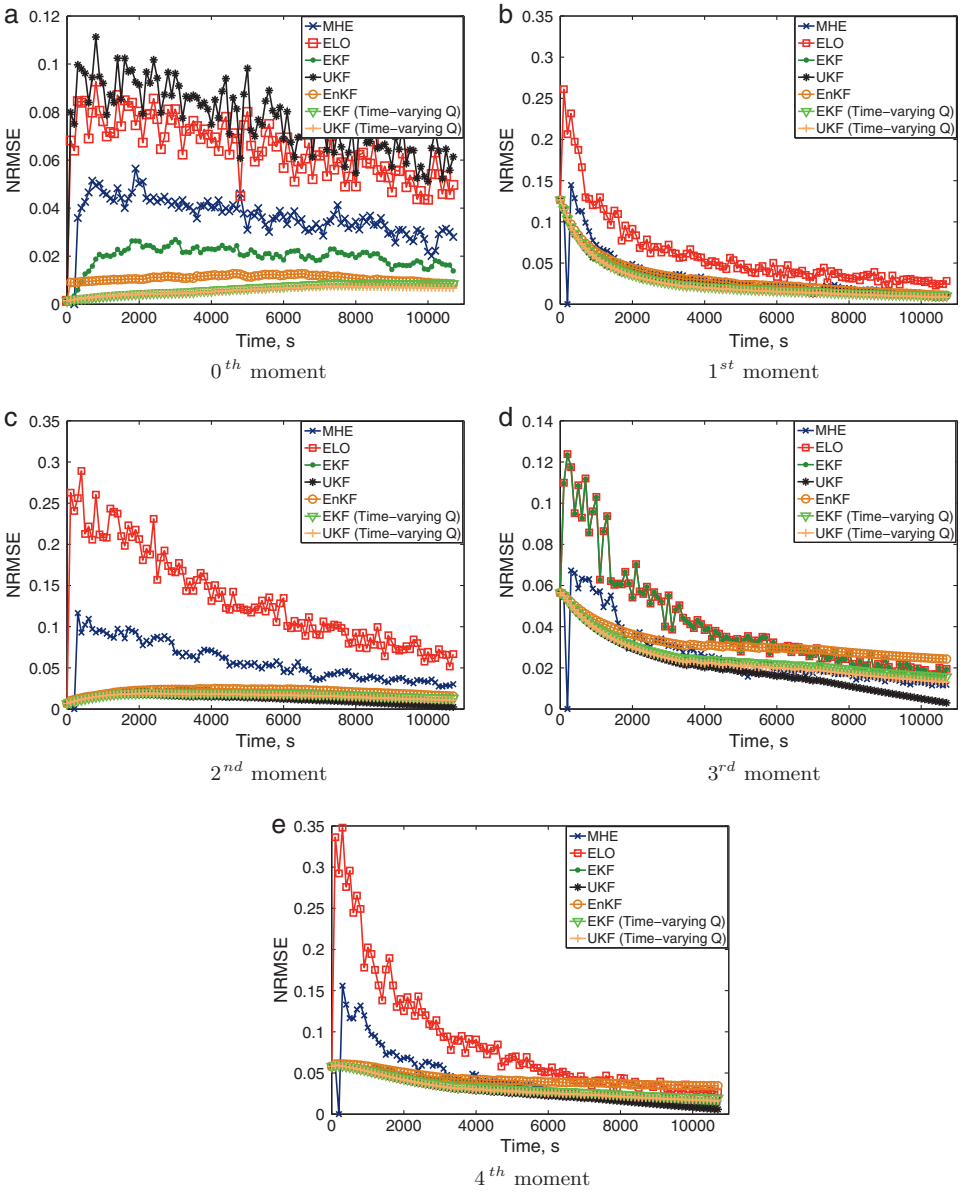

Fig. 3. State estimation errors under the open-loop scenario.

of batch throughput by tracking the maximum admissible crystal growth rate throughout the batch run. Note that the lower heat input bound $H_{\min}$ is to ensure the survival of ground seeds in the initial phase of the batch, whereas the upper heat input bound $H_{\max}$ is due to heat transfer limitations of the process. The optimal control problem is implemented in the Matlab toolbox OptCon [47], which uses the large-scale nonlinear optimization solver HQP [17].

The feedback control system depicted in Fig. 1 is used to continuously solve the optimal control problem in a receding horizon mode; d and ε denote the unmeasured process disturbances and the measurement errors, respectively. The observer plays a crucial role in this control strategy through estimating the system states at each sampling time interval when measurements y_{meas} become available. The estimated states $\hat{x}$ are used to recursively initialize the dynamic optimizer, which calculates the optimal operating policy of the crystallizer, i.e. u_{opt}. In addition, the observer allows us to estimate the solute concentration, for which measurements are not available.

In this study, the model-based control strategy is applied to a plant simulator that simulates the system using a process model having exactly the same structure as the model incorporated in the observer and the dynamic optimizer. The closed-loop performance of the control strategy, which is largely dependent on the quality of state estimates, is evaluated under the following scenarios:

- nominal case, where the measurements y_{meas} are corrupted by random noise sequences having normal distributions;
- uncertain case, which aims to examine how well the control objective, namely the reference crystal growth rate trajectory tracking, is fulfilled in the presence of model imperfections and process uncertainties.

The state estimation errors are expressed in terms of the normalized root mean squared error (NRMSE)

$$\text{NRMSE} = \sqrt{\mathbb{E}\left[\left(\frac{x(t)-\hat{x}(t)}{x(t)}\right)^2\right]}, \tag{27}$$

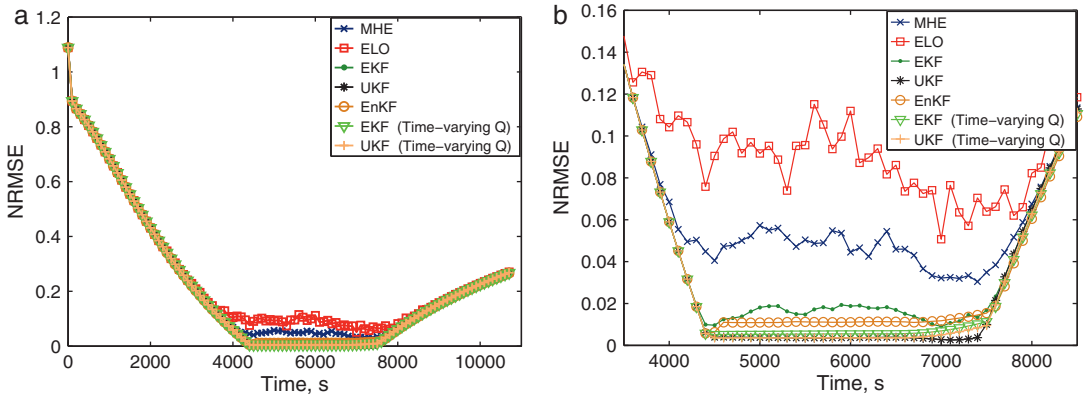

Throughout the entire batch time

Throughout the time frame over which the control objective is fulfilled

Fig. 4. Errors in the reference crystal growth rate trajectory tracking under the nominal scenario.

where $x(t)$ denotes the true system states obtained from the plant simulator. The expected values of the relative estimation errors are calculated based on 50 simulation runs. Similarly, the control performance is evaluated in terms of the reference trajectory tracking error defined as

$$\text{NRMSE} = \sqrt{\mathbb{E}\left[\left(\frac{G_{\max} - G(t)}{G_{\max}}\right)^2\right]}. \tag{28}$$

The nonlinear observers are implemented in Matlab. In the extended Luenberger observer, the set of continuous model equations is solved using the ODE15s function as it is capable of efficiently integrating highly stiff differential algebraic equations. On the other hand, the implicit Euler scheme is used in the stochastic observers to discretize the continuous model equations with a discretization time step of 5 s. The implicit Euler scheme is chosen due to its unconditional numerical stability. The moving horizon estimator is implemented in the Matlab toolbox OptCon [61,67]. In the moving horizon estimator, the process model is developed in C++. It is expected that the moving horizon estimator exhibits improved computational efficiency owing to the use of the compiled C++ model and solver libraries in the OptCon toolbox. The set of model equations is solved by the DASPK solver [8].

In the unscented Kalman filter, the sigma points are chosen symmetrically around the a priori state vector with a distance of the square root of the covariance, i.e. $\eta(\sqrt{P_{k+1|k}})_i$, where η is a scaling parameter [72]. On the other hand, the ensemble members in the ensemble Kalman filter are randomly drawn from a normal distribution around the a priori state vector. The stochastic filters are tuned such that more weight is attached to the process model since the measurement noise is rather large. The tuning parameters of the extended Luenberger observer are determined on the basis of an off-line optimization problem [43]. To have a fair performance evaluation, the tuning parameters of the observers remain fixed in the various scenarios unless otherwise stated. The tuning parameters are given in Appendix A.

3.3.1. Nominal scenario

Fig. 2 shows the estimation errors of the five leading moments of CSD under the nominal scenario. It is observed that the estimations made by the ELO and the MHE in the presence of stochastic measurement noise are of somewhat worse quality than those provided by the Kalman filters. This results from the deterministic estimation framework of the ELO and the elimination of the arrival cost term in the MHE. The arrival cost term is not well-defined for batch systems due to large variations of the state variables throughout the batch run. The omission of the arrival cost term reduces the Bayesian framework of the MHE to a deterministic optimization-based estimation technique. The integration of measurements over the estimation horizon in the MHE yet averages out the measurement noise to some degree. On the other hand, the better estimation quality of the UKF is attributed to its derivative free Bayesian frame-

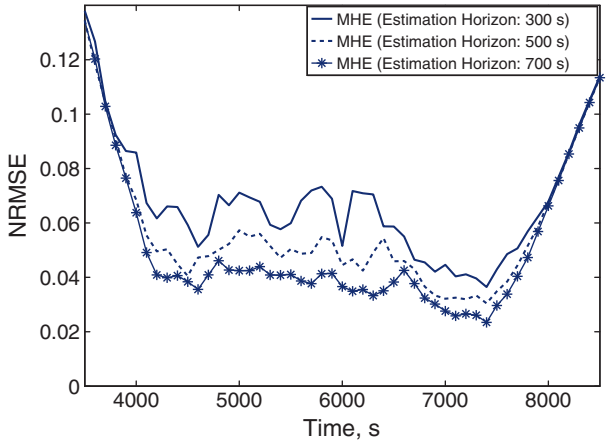

Fig. 5. Errors in the reference crystal growth rate trajectory tracking in relation to the estimation horizon of the MHE.

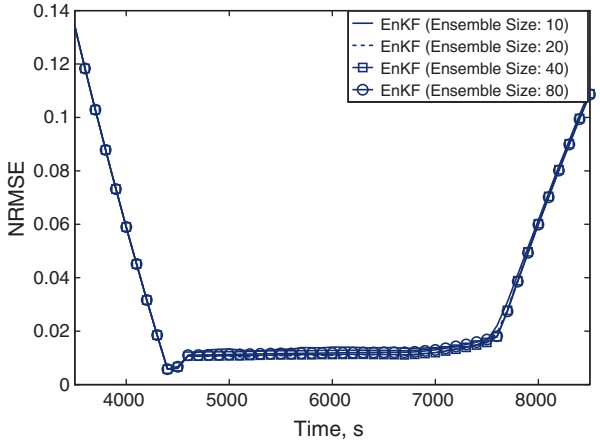

Fig. 6. Errors in the reference crystal growth rate trajectory tracking in relation to the ensemble size of the EnKF.

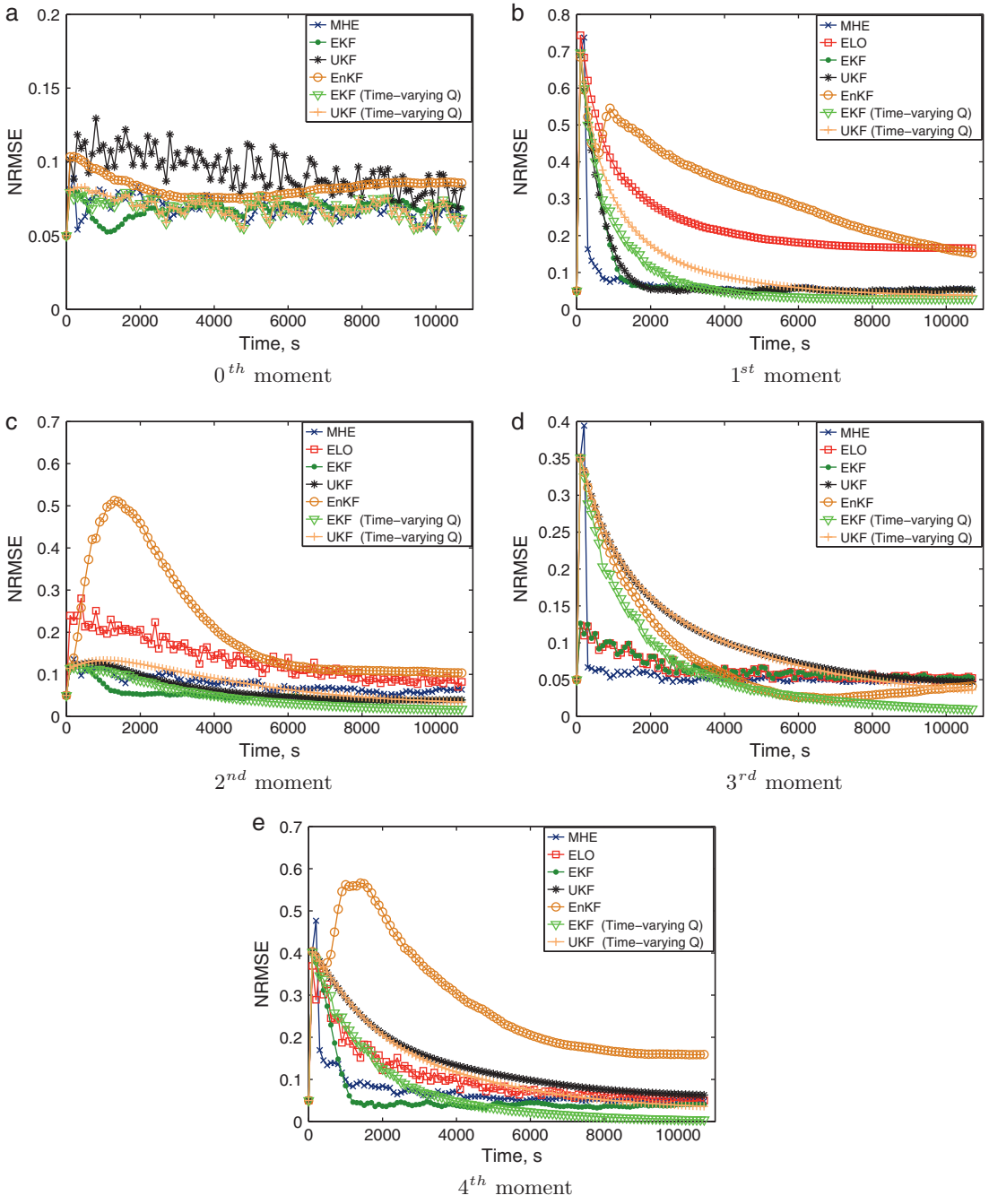

Fig. 7. State estimation errors under the uncertain scenario.

work. The latter estimation technique not only circumvents the need to approximate the nonlinear process model, but also allows us to effectively cope with the process stochasticity. Table 2 lists the computation times of the nonlinear observers implemented under the nominal scenario. As expected, the ELO, the EKF and the UKF have a comparable computational burden, while being considerably less than that of the MHE. It is evident that the computational efficiency of the nonlinear observers permits their online application given that the measurement sampling time is 100 s.

The performance of the nonlinear observers is also evaluated when the optimal heat input profile obtained under the nominal scenario is applied to the plant simulator in an open-loop mode. In the so-called open-loop scenario, the operating policy of the crystallizer is not computed on the basis of the state estimates. The open-loop state estimation errors of the observers are shown in Fig. 3. As can be seen, the error trends are similar to those obtained under the closed-loop scenario. However, the observers tend to have somewhat larger estimation errors and a slower convergence in the open-loop case.

To further improve the estimation quality of the EKF and the UKF, a tuning method that particularly suits batch processes is adopted [71]. Nagy and Braatz [48] demonstrated that the estimation accuracy of the EKF in the case of batch crystallization can be significantly improved using a time-varying process noise covariance matrix. In this approach, the information on model uncertainties is used to systematically calculate the process noise covariance matrix. The model uncertainties are specified on the basis of the parameter covariance matrix V_θ. The time-varying pro-

cess noise covariance matrix is defined as

$$Q(t) = \left(\frac{\partial \mathcal{F}}{\partial \theta}\right)_{x(t),u(t),\theta} V_\theta \left(\frac{\partial \mathcal{F}}{\partial \theta}\right)^T_{x(t),u(t),\theta}, \quad (29)$$

where the sensitivity matrix $\partial\mathcal{F}/\partial\theta$ is determined online. In this study, the parameter covariance matrix is obtained on the basis of the inference of model parameters from experimental data using the advanced statistical analysis tool of gPROMS [31]. The sensitivity matrix is calculated analytically owing to the low order of the system.

Eq. (29) indicates that the nondiagonal process noise covariance matrix is dependent on the current state of the dynamic system. Figs. 2 and 3 suggest that the latter approach leads to a rather significant improvement in the estimation accuracy of the EKF and the UKF, while the additional computation time for online calculation of $Q(t)$ is small (see Table 2). The calculated process noise covariance matrix varies largely along the batch time. Therefore, the use of a constant diagonal process noise covariance matrix obtained by trial and error tuning results in larger estimation errors.

Successful application of the model-based control strategy heavily relies on the information about states of the dynamic system. The degree, to which the state estimation accuracy affects the closed-loop performance of the model-based controller, is investigated. Fig. 4(a) displays the normalized root mean squared errors of the crystal growth rate with respect to its maximum admissible value, i.e. the reference trajectory (see Eq. (28)). The crystal growth rate is inferred from the solute concentration estimates provided by the observers. Due to the heat input constraints included in the optimal control problem [42], the control objective can only be fulfilled throughout a limited time horizon as shown in Fig. 4(b). A connection between the state estimation accuracy and the fulfillment of the control objective can be established by comparing the NRMSE of the crystal growth rate and that of the estimated states. Fig. 4(b) suggests that amongst the five leading moments of CSD, the closed-loop control performance is more closely connected to the estimation accuracy of the 2nd moment of CSD. As can be seen, the relatively poor state estimation by the ELO and the MHE leads to ineffective tracking of the reference trajectory. On the other hand, as expected, the Kalman filters allow the controller to more effectively follow the reference trajectory. This will result in a product with the desired quality attributes.

To enhance the closed-loop performance of the MHE, its estimation horizon is varied. Fig. 5 shows the reference trajectory tracking errors for different estimation horizons. As expected, the closed-loop performance of the MHE improves by extending the estimation horizon. This is however achieved at the expense of slightly higher computational costs (see Table 2). The effect of the ensemble size N on the closed-loop performance of the EnKF is also investigated. The appropriate number of ensemble members is typically determined on the basis of the state dimension and the nonlinearity of the system. The errors in the reference trajectory tracking in relation to ensemble size $N = 10$, 20, 40 and 80 are shown in Fig. 6. As can be seen, the errors decrease as the ensemble size is doubled from 10 to 20. However, further improvement in the closed-loop control performance cannot be achieved by increasing the ensemble size N once a threshold size of 20 is reached. Table 2 indicates that the computational burden of the EnKF increases approximately linearly with respect to the number of ensemble members.

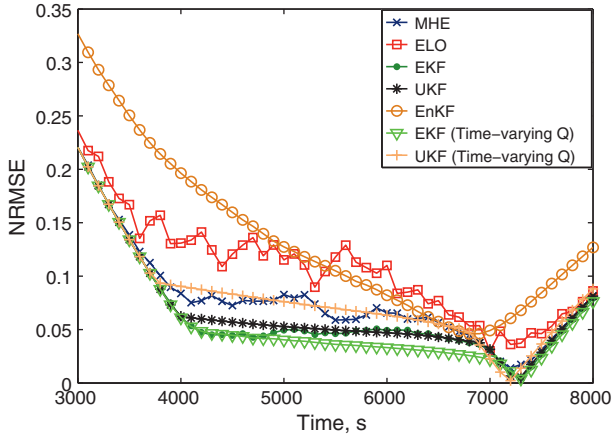

Fig. 8. Errors in the reference crystal growth rate trajectory tracking under the uncertain scenario.

Table 3
Specifications of model imperfection and process uncertainties in the uncertain scenario.

Parametric plant-model mismatch	+35.0% error in k_b and k_g
Systematic measurement error	+5.0% error in the five leading moments of CSD
Uncertain initial conditions	+2.0% error in the initial concentration +5.0% error in the five leading moments of the initial CSD

3.3.2. Uncertain scenario

Industrial batch crystallizers are typically prone to various process uncertainties, mainly arisen from measurement deficiencies and uncertain initial conditions due to improper seeding. In addition, the great degree of uncertainty often associated with the parameters of crystallization kinetic models may not allow the process model to provide an adequate description of the system dynamics. The capability of nonlinear observers in coping with model imperfections and process disturbances is examined under a scenario with uncertainty specifications given in Table 3. The EKF and the UKF with time-varying process noise covariance matrix as well as the EnKF are retuned to avoid divergence, which is primarily caused by the introduction of plant-model mismatch. When more weight is attached to the process model, the observers tend to diverge in the presence of plant-model mismatch due to inaccurate description of the system dynamics. The divergence can be compensated for by attaching more weight to the information obtained from the plant simulator.

Fig. 7 shows the estimation errors of the five leading moments of CSD under the uncertain scenario. It is observed that the initial estimation errors are not zero due to the discrepancy between the initial conditions of the process model and those of the plant simulator. In comparison with the nominal scenario, the latter effect leads to larger estimation errors in the initial phase of the batch. As the system evolves in time, the observability of the system allows the large initial estimation errors to vanish and converge to values comparable to those achieved under the nominal scenario. In addition, Fig. 7 suggests that the estimation errors tend to stabilize around larger values than in the nominal scenario. This is attributed to the systematic measurement error, which introduces a bias in the state estimates. As can be seen, the EnKF cannot adequately cope with process uncertainties and model imperfections, whereas the EKF, the UKF and the MHE exhibit a significantly better performance. Likewise the nominal scenario, the EKF and the UKF with time-varying process noise covariance matrix give better estimation accuracy and faster convergence rates, in particular for the higher moments of CSD.

The errors in the reference crystal growth rate trajectory tracking under the uncertain scenario are shown in Fig. 8. The bias in the state estimates, particularly in the 2nd moment of CSD, has deteriorated the closed-loop performance of the controller by introducing an off-set in the reference trajectory tracking. This is due to the

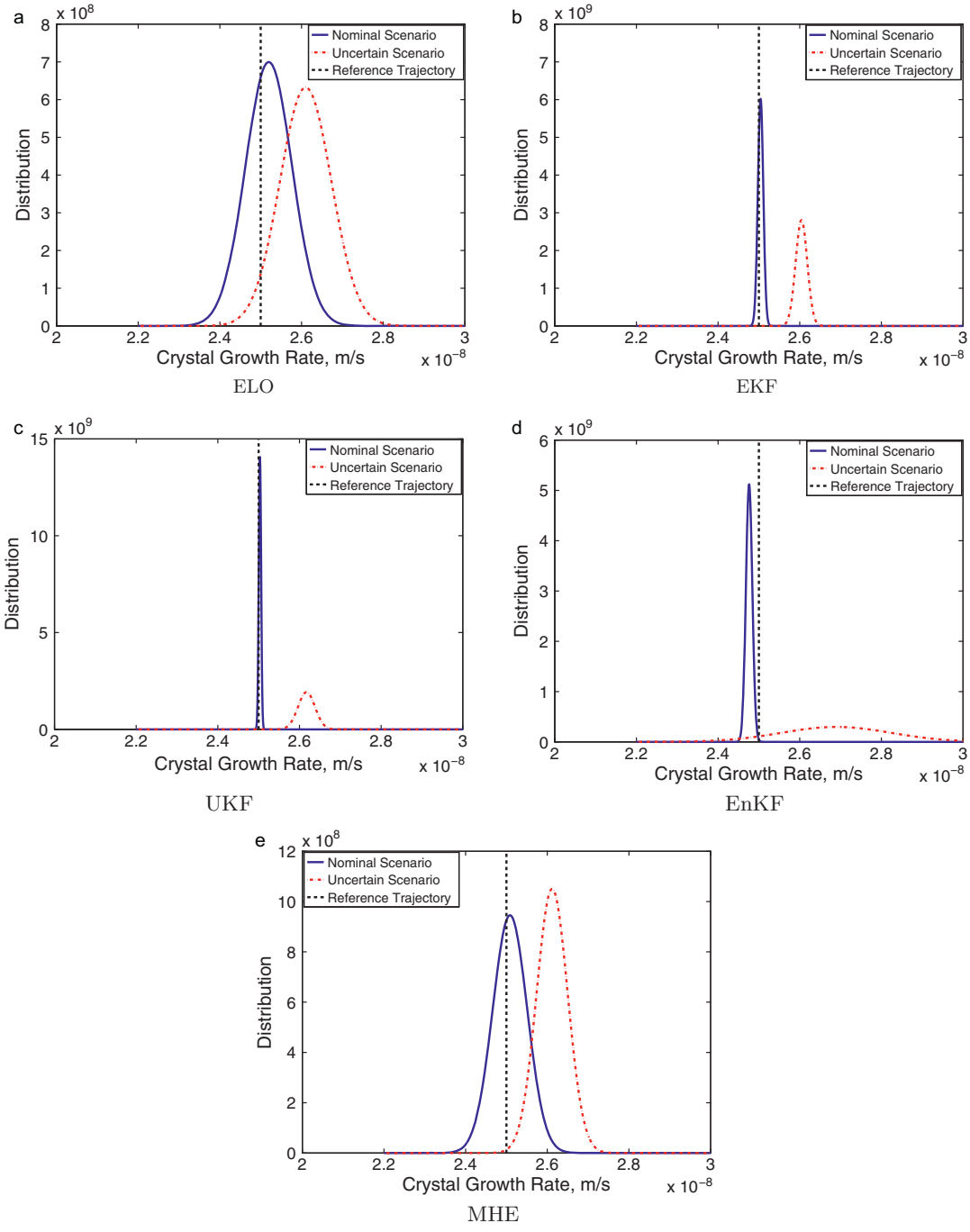

Fig. 9. The normal probability distribution of the crystal growth rates inferred by the nonlinear observers.

inability of the observers to effectively deal with parametric model imperfections and systematic measurement errors. Fig. 9 depicts the normal probability distribution of crystal growth rates inferred under the nominal and uncertain scenarios; the dashed line represents the maximum admissible crystal growth rate. It is observed that the crystal growth rates obtained under the uncertain scenario exhibit a rather large deviation with respect to the reference trajectory. The violation of the maximum admissible crystal growth rate may significantly degrade the product quality due to, e.g. formation of irregularly shaped crystals and impurity uptakes, even though higher crystal growth rates will result in increased batch productivity. Fig. 9 indicates that the EKF and the UKF possess the narrowest distributions under both scenarios. The ability of the latter filters in providing accurate state estimates under the nominal scenario enables the controller to satisfactorily fulfill its objective.

The closed-loop control performance under the uncertain scenario is enhanced by including a disturbance model into the nonlinear observers. As the performance of the controller is closely connected to the estimation accuracy of the 2nd moment of CSD, the disturbance model primarily aims to eliminate the off-set in the estimates of the latter state variable. Hence, an extra state variable with a constant value is augmented to the state vector to estimate and subsequently suppress the disturbances acting on m_2. Fig. 10 suggests that the disturbance model incorporated into the EKF and the UKF significantly enhances the estimation accuracy of the 2nd moment of CSD. Fig. 11 depicts the optimal crystal growth rate profiles throughout the batch run. It is evident that the disturbance

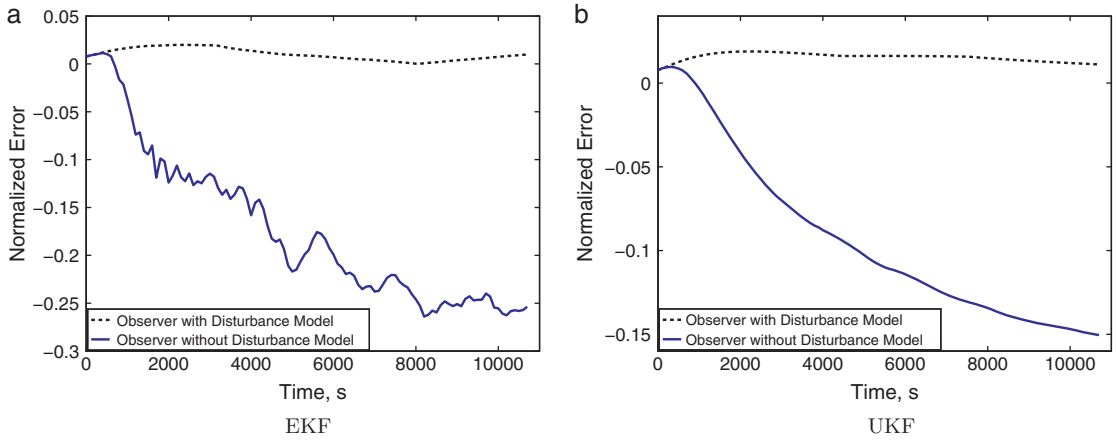

Fig. 10. Normalized estimation errors of the 2nd moment of CSD under the uncertain scenario.

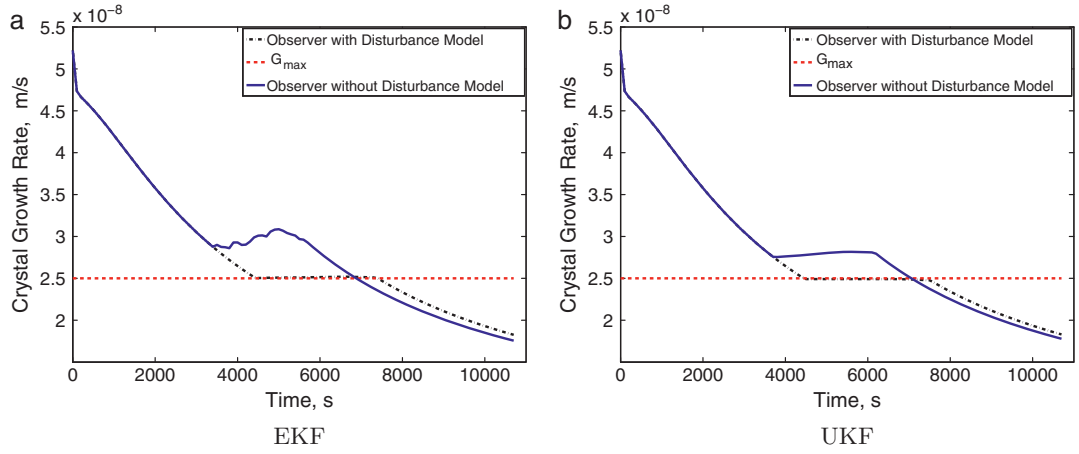

Fig. 11. The optimal crystal growth rate profiles under the uncertain scenario.

model adequately describes the disturbances acting on the system and consequently enables effective reference trajectory tracking in the time frame, over which the control objective can be fulfilled. As can be seen, the model-based controller fails to tightly follow the reference trajectory when the disturbance model is not incorporated into the EKF and the UKF. Note that the maximum crystal growth rate cannot be maintained in the initial and the final phases of the batch run due to actuation limitations.

4. Conclusions

In this paper, several nonlinear observers developed under deterministic and Bayesian estimation frameworks have been applied for output feedback model-based control of a semi-industrial fed-batch crystallizer. The dynamics of the process at hand are described by a computationally affordable reduced order moment model derived from the population balance equation. The observability analysis of the nonlinear system verifies that the unmeasurable process variable, namely the solute concentration, can be estimated from the online crystal size distribution measurements. The availability of solute concentration estimations is essential for the control application under study.

The closed-loop simulation results of the model-based controller when applied to a plant simulator indicate that the ELO and the MHE cannot adequately suppress the stochastic measurement noise. This results from the deterministic framework of the ELO and the elimination of the arrival cost term in the MHE, which is not often well-defined in batch crystallization processes. On the other hand, the stochastic observers, in particular the UKF, provide accurate state estimations that ensure satisfactory closed-loop control performance. The better estimation accuracy of the UKF is due to its derivative free Bayesian framework that circumvents the need to approximate the nonlinear model. The estimation accuracy of the stochastic observers can be further improved by adopting a time-varying process noise covariance matrix, which is dependent on the current state of the dynamic system. This approach is particularly suitable for batch crystallization processes as the system states and consequently the process noise covariance matrix vary largely throughout the batch run. The simulation results suggest that the model-based controller fails to adequately fulfill its objective in the presence of model imperfections and process uncertainties. This is due to the inability of the nonlinear observers to provide accurate state estimates. It is demonstrated that the closed-loop performance of the controller can be enhanced by incorporating a disturbance model into the observers.

Acknowledgments

The work presented in this paper was carried out within the EUREKA/IS-project E! 3458/IS043074, called CryPTO (Crystallizer based Processing: fundamenTal research into mOdelling). The financial support of SenterNovem is gratefully acknowledged. The authors thank Israel Mora Moreno for his contribution to this study.

Appendix A.

The tuning parameters of the nonlinear observers applied in the nominal scenario are given in this appendix.

A.1. Extended Luenberger observer

Observer gain:

$$K_k = \begin{bmatrix} 0 & 0 & 0 & 2.72\times10^{-3} & 0 \\ 0 & 0 & 0 & 0 & 8.45\times10^{1} \\ 0 & 0 & 1.17\times10^{-1} & 0 & 0 \\ 0 & 0 & 0 & 4.41\times10^{-1} & 0 \\ 0 & 0 & 0 & 0 & 4.64\times10^{-1} \\ 0 & 0 & 0 & 0 & 0 \end{bmatrix} \quad (30)$$

A.2. Extended Kalman filter

Process noise covariance matrix:

$$Q_k = \begin{bmatrix} 45\times10^{20} & 0 & 0 & 0 & 0 & 0 \\ 0 & 27\times10^{8} & 0 & 0 & 0 & 0 \\ 0 & 0 & 9\times10^{-2} & 0 & 0 & 0 \\ 0 & 0 & 0 & 90 & 0 & 0 \\ 0 & 0 & 0 & 0 & 9\times10^{-9} & 0 \\ 0 & 0 & 0 & 0 & 0 & 45\times10^{-4} \end{bmatrix} \quad (31)$$

Measurement noise covariance matrix:

$$R_k = \begin{bmatrix} 45\times10^{12} & 0 & 0 & 0 & 0 \\ 0 & 27\times10^{2} & 0 & 0 & 0 \\ 0 & 0 & 9 & 0 & 0 \\ 0 & 0 & 0 & 56\times10^{-13} & 0 \\ 0 & 0 & 0 & 0 & 63\times10^{-16} \end{bmatrix} \quad (32)$$

In the extended Kalman filter with time-varying process noise covariance matrix, the measurement noise covariance matrix remains the same as above.

A.3. Unscented Kalman filter

Process noise covariance matrix:

$$Q_k = \begin{bmatrix} 45\times10^{18} & 0 & 0 & 0 & 0 & 0 \\ 0 & 27\times10^{8} & 0 & 0 & 0 & 0 \\ 0 & 0 & 9\times10^{-2} & 0 & 0 & 0 \\ 0 & 0 & 0 & 9\times10^{-1} & 0 & 0 \\ 0 & 0 & 0 & 0 & 9\times10^{-5} & 0 \\ 0 & 0 & 0 & 0 & 0 & 4\times10^{-7} \end{bmatrix} \quad (33)$$

Measurement noise covariance matrix:

$$R_k = \begin{bmatrix} 9\times10^{9} & 0 & 0 & 0 & 0 \\ 0 & 81\times10^{4} & 0 & 0 & 0 \\ 0 & 0 & 9\times10^{-5} & 0 & 0 \\ 0 & 0 & 0 & 9\times10^{-1} & 0 \\ 0 & 0 & 0 & 0 & 9\times10^{-5} \end{bmatrix} \quad (34)$$

In the unscented Kalman filter with time-varying process noise covariance matrix, the measurement noise covariance matrix remains the same as above.

A.4. Ensemble Kalman filter

In the ensemble Kalman filter with 20 ensemble members, the noise added to the observation is drawn from a zero-mean normal distribution with variances given by

$$R_k = \begin{bmatrix} 3\times10^{17} & 0 & 0 & 0 & 0 \\ 0 & 27\times10^{9} & 0 & 0 & 0 \\ 0 & 0 & 3\times10^{5} & 0 & 0 \\ 0 & 0 & 0 & 3\times10^{4} & 0 \\ 0 & 0 & 0 & 0 & 30 \end{bmatrix}. \quad (35)$$

References

[1] S. Arulampalam, S. Maskell, N. Gordon, T. Clapp, A tutorial on particle filters for online nonlinear/non-Gaussian Bayesian tracking, IEEE Transactions on Signal Processing 50 (2002) 174–188.
[2] T. Bakir, S. Othman, G. Fevotte, H. Hammouri, Nonlinear observer of crystal-size distribution during batch crystallization, AIChE Journal 52 (2006) 2188–2197.
[3] G. Bastin, D. Dochain, On-line Estimation and Adaptive Control of Bioreactors, Elsevier, Amsterdam, 1990.
[4] S. Biagiola, J. Figueroa, Application of state estimation based NMPC to an unstable nonlinear process, Chemical Engineering Science 59 (2004) 4601–4612.
[5] S. Biagiola, J. Solsona, State estimation in batch processes using a nonlinear observer, Mathematical and Computer Modelling 44 (2006) 1009–1024.
[6] P. Bogaerts, A hybrid asymptotic-Kalman observer for bioprocesses, Bioprocess Engineering 20 (1999) 101–113.
[7] R. Braatz, Advanced control of crystallization processes, Annual Reviews in Control 26 (2002) 87–99.
[8] P. Brown, A. Hindmarsh, L. Petzold, Using krylov methods in the solution of large-scale differential algebraic systems, SIAM Journal Scientific Computing 15 (1994) 1467–1488.
[9] G. Burgers, P. Leeuwen, G. Evensen, Analysis scheme in the ensemble Kalman filter, Monthly Weather Review 126 (1998) 1719–1724.
[10] T. Chen, J. Morris, E. Martin, Particle filters for state and parameter estimation in batch processes, Journal of Process Control 15 (2005) 665–673.
[11] G. Ciccarella, M.D. Mora, A. Germani, A luenberger-like observer for nonlinear systems, International Journal of Control 57 (1993) 537–556.
[12] P. Daudey, G. van Rosmalen, E.D. Jong, Secondary nucleation kinetics of ammonium sulphate in a cmsmpr crystallizer, Journal of Crystal Growth 99 (1990) 1076–1081.
[13] F. Daum, Nonlinear filters: beyond the Kalman filter, IEEE A&E Systems Magazine 20 (2005) 57–69.
[14] F. Deza, D. Bossanne, E. Busvelle, J. Gauthier, D. Rakotopara, Exponential observers for nonlinear systems, IEEE Transactions on Automatic Control 38 (1993) 482–484.
[15] D. Dochain, State and parameter estimation in chemical and biochemical processes: a tutorial, Journal of Process Control 13 (2003) 801–818.
[16] G. Evensen, Advanced data assimilation for strongly nonlinear dynamics, Monthly Weather Review 125 (1997) 1342–1354.
[17] R. Franke, E. Arnold, H. Linke, HQP: a solver for nonlinearly constrained optimization, 2005. http://hqp.sourceforge.net.
[18] E. Gatzke, F. Doyle, Use of multiple models and qualitative knowledge for online moving horizon disturbance estimation and fault diagnosis, Journal of Process Control 12 (2002) 339–352.
[19] J. Gauthier, A. Kupka, Observability and observers for nonlinear systems, SIAM Journal on Control and Optimization 32 (1992) 975–994.
[20] S. Gillijns, O.B. Mendoza, J. Chandrasekar, B.D. Moor, D. Bernstein, A. Ridley, What is the ensemble Kalman filter and how well does it work? in: Proceedings of the American Control Conference, Minnesota, USA, 2006, pp. 4448–4453.
[21] N. Gordon, D. Salmond, A. Smith, Novel approach to nonlinear/non-Gaussian Bayesian state estimation IEE Proceedings F-Radar and Signal Processing 140 (1993) 107–113.
[22] Y. Hao, Z. Xiong, F. Sun, X. Wang, Comparison of unscented Kalman filters, in: Proceedings of IEEE International Conference on Mechatronics and Automation, Harbin, China, 2007, pp. 895–899.
[23] E. Haseltine, J. Rawlings, Critical evaluation of extended Kalman filtering and moving-horizon estimation, Industrial and Engineering Chemistry Research 44 (2005) 2451–2460.
[24] M. Hermanto, M. Chiu, R. Braatz, Nonlinear model predictive control for the polymorphic transformation of L-glutamic acid crystals, AIChE Journal 55 (2009) 2631–2645.
[25] P. Houtekamer, H. Mitchell, Ensemble Kalman filtering, The Quarterly Journal of the Royal Meteorological Society 131 (2005) 3269–3290.
[26] X. Hulhoven, A.V. Wouwer, P. Bogaerts, Hybrid extended Luenberger-asymptotic observer for bioprocess state estimation, Chemical Engineering Science 61 (2006) 7151–7160.
[27] J. Jansen, O. Bosgra, P.V. den Hof, Model-based control of multiphase flow in subsurface oil reservoirs, Journal of Process Control 18 (2008) 846–855.
[28] S. Julier, J. Uhlmann, A new extension of the Kalman filter to nonlinear systems, in: Proceedings of the 11th International Symposium on Aerospace/Defense Sensing, Simulation and Controls, Orlando, USA, 1997, pp. 182–193.
[29] S. Julier, J. Uhlmann, Unscented filtering and nonlinear estimation, Proceedings of the IEEE 92 (2004) 401–422.
[30] S. Kadam, E. van der Windt, P. Daudy, H. Kramer, A comparative study of ATR-FTIR and FT-NIR spectroscopy for the in-situ concentration monitoring during batch cooling crystallization processes, Crystal Growth & Design 10 (2010) 2629–2640.
[31] A. Kalbasenka, Model-based control of industrial batch crystallizers: experiments on enhanced controllability by seeding actuation. Ph.D. Thesis, Delft University of Technology, The Netherlands, 2009.
[32] A. Kalbasenka, L. Spierings, A. Huesman, H. Kramer, Application of seeding as a process actuator in a model predictive control framework for fed-batch crystallization of ammonium sulphate, Particle and Particle Systems Characterization 24 (2007) 40–48.
[33] R. Kalman, R. Bucy, New results in linear filtering and prediction, Journal of Basic Engineering (ASME) 83 (1961) 98–108.

[34] R. Kandepu, B. Foss, L. Imsland, Applying the unscented Kalman filter for nonlinear state estimation, Journal of Process Control 18 (2008) 753–768.
[35] A. Krener, A. Isidori, Linearization by output injection and nonlinear observers, Systems and Control Letters 3 (1983) 47–52.
[36] J. Landlust, A. Mesbah, J. Wildenberg, A. Kalbasenka, H. Kramer, J. Ludlage, An industrial model predictive control architecture for batch crystallization, in: Proceedings of the 17th International Symposium on Industrial Crystallization, Maastricht, The Netherlands, 2008, pp. 35–42.
[37] J. Lee, L. Ricker, Extended Kalman filter based nonlinear model predictive control, Industrial and Engineering Chemistry Research 33 (1994) 1530–1541.
[38] K. Lee, J. Lee, D. Yang, A. Mahoney, Integrated run-to-run and on-line model based control of particle size distribution for a semi-batch precipitation reactor, Computers and Chemical Engineering 26 (2002) 1117–1131.
[39] V. Lemesle, J. Gouze, A bounded error observer for a class of bioreactor models, in: Proceedings of the 8th IFAC Conference on Computer Applications in Biotechnology (CAB8), Quebec, Canada, 2001, pp. 24–27.
[40] M. Leskens, L. van Kessel, P.V. den Hof, O. Bosgra, Nonlinear model predictive control with moving horizon state and disturbance estimation with application to MSW combustion, in: Proceedings of the 16th IFAC World Congress, Prague, Czech Republic, 2005.
[41] M. Mangold, A. Buck, R. Schenkendorf, C. Steyer, A. Voigt, K. Sundmacher, Two state estimators for the barium sulfate precipitation in a semi-batch reactor, Chemical Engineering Science 64 (2009) 646–660.
[42] A. Mesbah, A. Huesman, H. Kramer, Z. Nagy, P.V. den Hof, Real-time control of a semi-industrial fed-batch evaporative crystallizer using different direct optimization strategies. AIChE Journal, doi:10.1002/aic.12366.
[43] A. Mesbah, A. Kalbasenka, A. Huesman, H. Kramer, P.V. den Hof, Real-time dynamic optimization of batch crystallization processes, in: Proceedings of the 17th IFAC World Congress, Seoul, Korea, 2008, pp. 3246–3251.
[44] A. Mesbah, J. Landlust, A. Huesman, H. Kramer, P. Jansens, P.V. den Hof, A model-based control framework for industrial batch crystallization processes, Chemical Engineering Research and Design 88 (2010) 1223–1233.
[45] S. Motz, S. Mannal, E. Gilles, State estimation in batch crystallization using reduced population models, Journal of Process Control 18 (2008) 361–374.
[46] Z. Nagy, Model based robust control approach for batch crystallization product design, Computers and Chemical Engineering 33 (2009) 1685–1691.
[47] Z. Nagy, F. Allgower, R. Franke, A. Frick, B. Mahn, Efficient tool for nonlinear model predictive control of batch processes, in: Proceedings of the 12th Mediterranean Conference on Control and Automation, Kusadasi, Turkey, 2004.
[48] Z. Nagy, R. Braatz, Robust nonlinear model predictive control of batch processes, AIChE Journal 49 (2003) 1776–1786.
[49] Z. Nagy, B. Mahn, R. Franke, F. Allgower, Evaluation study of an efficient output feedback nonlinear model predictive control for temperature tracking in an industrial batch reactor, Control Engineering Practice 15 (2007) 839–850.
[50] A. Neumann, H. Kramer, A comparative study of various size distribution measurement systems, Particle & Particle Systems Characterization 19 (2002) 17–27.
[51] H. Nijmeijer, A. van der Schaft, Nonlinear Dynamical Control Systems, Springer, New York, 1990.
[52] R. Oliveira, E. Ferreira, S.F. de Azevedo, Stability dynamics of convergence and tuning of observer-based kinetic estimators, Journal of Process Control 12 (2002) 311–323.
[53] M. Perrier, S.F. de Azevedo, E. Ferreira, D. Dochain, Tuning of observer-based estimators: theory and application to the on-line estimation of kinetic parameters, Control Engineering Practice 8 (2000) 377–388.
[54] J. Prakash, S. Patwardhan, S. Shah, Constrained state estimation using the ensemble Kalman filter, in: Proceedings of the American Control Conference, Seattle, USA, 2008, pp. 3542–3547.
[55] C. Qu, J. Hahn, Process monitoring and parameter estimation via unscented Kalman filtering, Journal of Loss Prevention in the Process Industries 22 (2009) 703–709.
[56] A. Randolph, M. Larson, Theory of Particulate Processes, 2nd ed., Academic Press, San Diego, 1988.
[57] C. Rao, J. Rawlings, Constrained process monitoring: moving-horizon approach, AIChE Journal 48 (2002) 97–109.
[58] C. Rao, J. Rawlings, D. Mayne, Constrained state estimation for nonlinear discrete-time systems: Stability and moving horizon approximations, IEEE Transactions on Automatic Control 48 (2003) 246–258.
[59] J. Rawlings, B. Bakshi, Particle filtering and moving horizon estimation, Computers and Chemical Engineering 30 (2006) 1529–1541.
[60] D. Robertson, J. Lee, J. Rawlings, A moving horizon-based approach for least-squares state estimation, AIChE Journal 42 (1996) 2209–2224.
[61] R. Roman, Z. Nagy, M. Cristea, S. Agachi, Dynamic modelling and nonlinear model predictive control of a fluid catalytic cracking unit, Computers and Chemical Engineering 33 (2009) 605–617.
[62] A. Romanenko, J. Castro, The unscented filter as an alternative to the EKF for nonlinear state estimation: a simulation case study, Computers and Chemical Engineering 28 (2004) 347–355.
[63] A. Romanenko, L. Santos, P. Afonso, Unscented Kalman filtering of a simulated pH system, Industrial and Engineering Chemistry Research 43 (2004) 7531–7538.
[64] D. Rozier, F. Birol, E. Cosme, P. Brasseur, J. Brankart, J. Verron, A reduced order Kalman filter for data assimilation in physical oceanography, SIAM Review 49 (2007) 449–465.
[65] T. Schei, On-line estimation for process control and optimization applications, Journal of Process Control 18 (2008) 821–828.
[66] D. Shi, P. Mhaskar, N. El-Farra, P. Christofides, Predictive control of crystal size distribution in protein crystallization, Nanotechnology 16 (2005) S562–S574.
[67] L. Simon, Z. Nagy, K. Hungerbuhler, Model based control of a liquid swelling constrained batch reactor subject to recipe uncertainties, Chemical Engineering Journal 153 (2009) 151–158.
[68] M. Soroush, State and parameter estimations and their applications in process control, Computers and Chemical Engineering 23 (1998) 229–245.
[69] M. Srinivasarao, S. Patwardhan, R. Gudi, From data to nonlinear predictive control. 2. Improving regulatory performanace using identified observers, Industrial and Engineering Chemistry Research 45 (2006) 3593–3603.
[70] M. Tenny, J. Rawlings, Efficient moving horizon estimation and nonlinear model predictive control, in: Proceedings of the American Control Conference, 2002, pp. 4475–4480.
[71] J. Valappil, C. Georgakis, Systematic estimation of state noise statistics for extended Kalman filters, AIChE Journal 46 (2000) 292–308.
[72] R. van der Merwe, E. Wan, The square-root unscented Kalman filter for state and parameter estimation, in: Proceedings of IEEE International Conference on Acoustics, Speech and Signal Processing, Salt Lake City, USA, 2001, pp. 3461–3464.
[73] D. Wilson, M. Agarwal, D. Rippin, Experiences implementing the extended Kalman filter on an industrial batch reactor, Computers and Chemical Engineering 22 (1998) 1653–1672.
[74] W. Xie, S. Rohani, A. Phoenix, Extended Kalman filter based nonlinear geometric control of a seeded batch cooling crystallizer, Canadian Journal of Chemical Engineering 80 (2002) 167–172.
[75] M. Zeitz, Extended Luenberger observer for nonlinear systems, Systems and Control Letters 9 (1987) 149–156.
[76] G. Zhang, S. Rohani, On-line optimal control of a seeded batch cooling crystallizer, Chemical Engineering Science 58 (2003) 1887–1896.